Supporting Online Material for

Activation of Visual Pigments by Light and Heat

Dong-Gen Luo,* Wendy W. S. Yue, Petri Ala-Laurila, King-Wai Yau*

*To whom correspondence should be addressed. E-mail: dgluo@jhmi.edu (D.-G.L.);
kwyau@mail.jhmi.edu (K.-W.Y.)

This PDF file includes:

Materials and Methods
Figs. S1 to S9
Tables S1 to S5
References

Supporting Online Material

MATERIALS AND METHODS

Suction-pipette recording. Larval tiger salamander (*Ambystoma tigrinum*), toad (*Bufo marinus*), goldfish (*Carassius auratus*), and mouse (typically C57BL/6) were used. An animal was dark-adapted overnight, euthanized, and the eyes removed and hemisected under infrared light. The eyecups were stored in the respective Ringer (all species except mouse) or L-15 medium (mouse) on ice until use over many hours. When needed, a small piece was cut from the eyecup, and the retina removed, chopped, and transferred to the recording chamber perfused with Ringer [for toad/salamander: (in mM) 111 NaCl, 2.5 KCl, 1.6 $MgCl_2$, 1 $CaCl_2$, and 10 HEPES, pH 7.8, 0.02 EDTA, and 10 glucose; for goldfish: (in mM) 130 NaCl, 2.6 KCl, 1 $MgCl_2$, 1 $CaCl_2$, 10 HEPES, pH 7.8, 0.02 EDTA] or Locke's solution [for mouse: (in mM) 112.5 NaCl, 3.6 KCl, 2.4 $MgCl_2$, 1.2 $CaCl_2$, 10 HEPES, pH 7.4, 0.02 EDTA, 20 $NaHCO_3$, 3 Na_2-succinate, 0.5 Na-glutamate, 10 glucose, 0.1% vitamins (Sigma-Aldrich), and 0.1% amino-acid supplement (Sigma-Aldrich), bubbled with 95% O_2/5% CO_2]. Single-cell recordings were made under infrared light by drawing the outer segment of an isolated rod or cone (all species except mouse), or of a rod projecting from a fragment of retina (mouse), into a tight-fitting glass pipette containing one of the respective solutions above and connected to an Axopatch 200B amplifier. For mouse, the pipette solution contained (in mM): 140 NaCl, 3.6 KCl, 2.4 $MgCl_2$, 1.2 $CaCl_2$, 3 HEPES, pH 7.4, 0.02 EDTA, and 10 glucose. All signals were low-pass filtered at 20 Hz (8-pole Bessel) and sampled at 500 Hz, unless specified otherwise. Cell identification was based on morphology and spectral sensitivity.

Light stimulation was mostly with 10-ms, monochromatic flashes (30-60 repeated trials for dim flashes, and fewer for brighter ones, unless specified otherwise). The perfusion solution, with temperature monitored by a thermistor situated within 200 μm from the recorded cell, was warmed or cooled by passing through a heater or an ice enclosure. It took ~90 min to complete a set of stable spectral-sensitivity measurements at one temperature. Accordingly, recordings at different temperatures were made from different cells.

Effect of temperature on the absorption/action spectrum of a visual pigment. Fig. S1 shows diagrammatically the absorption spectrum of a visual pigment, plotted as logarithmic absorption (or sensitivity) against the reciprocal of normalized wavelength, λ_{max}/λ, which is proportional to photon energy. Plotted as such, the spectrum shows a linear descent at long λ (i.e., toward the far red) (*1-6*). Stiles (*3*) was the first to point out that this linear descent is consistent with the notion of thermal energy contributing to light absorption when the photon energy alone is insufficient for overcoming the minimum photoactivation energy, E_a^P [Stiles' theory was reproduced in (*4*)]. Based on this idea, light absorption at long wavelengths should increase at a higher temperature because the percentage of pigment molecules with sufficient complementary thermal energy for photoactivation is higher. This temperature effect has indeed been observed (*4, 7-10*). At shorter wavelengths, on the other hand, the photon energy itself is already sufficient, thus not requiring any thermal energy, and the temperature effect should disappear. The transition point, where the temperature effect starts to disappear, corresponds to the critical

wavelength, λ_c, with photon energy equal to E_a^P. St. George (*8*) reported that temperature may also change the quantum efficiency of isomerization. However, this was not observed by one of the authors here (*11*).

In our temperature-change experiments, we did not observe at a higher temperature a change in the relative sensitivity at $\lambda < \lambda_c$ (where $\lambda_c \sim \lambda_{max}/0.84$; see Main Text). Ala-Laurila *et al.* (*12*), on the other hand, reported a small decrease in relative sensitivity at $\lambda < \lambda_c$ (albeit only for a short range of λ), as well as a small blue shift in λ_{max}, at a higher temperature. Interestingly, they found these weak temperature effects only for red rods (which have rhodopsin), but not for green rods (which have blue cone pigment, see **Immunocytochemical labeling of blue cone pigment in *Bufo* green rods** below). A blue shift in λ_{max} at a higher temperature (0.03 – 0.06 nm/°C) was also reported by others for rhodopsin and iodopsin (*8, 13, 14*). The significance or meaning of these effects is unclear, as is their specificity to certain pigments. Because we did not observe these effects in our experiments (~10°C change in temperature), and because the plot of $\Delta\log_{10}$ (Normalized Sensitivity) versus λ_{max}/λ gave a reasonably linear relation almost up to the zero-change line (see Text Fig. 1 and 2), our estimate of λ_c is probably fairly reliable.

Estimation of λ_{max}/λ_c for larval salamander rods. In vertebrates, the chromophore in visual pigments is a vitamin-A derivative that is either 11-*cis*-retinal (A_1) for land and marine animals or 11-*cis*-3-dehydroretinal (A_2) for many aquatic species (*15*), covalently linked to the protein moiety, opsin, by a typically protonated Schiff base. For a given opsin, A_2 chromophore gives a longer λ_{max} than A_1 chromophore (*15*). Larval salamander "red" rods have mixed A_1 and A_2 rhodopsins, with the percentage of A_2 being around 52-72% (*16, 17*). However, because of the steep descent of a spectrum in the far red, and because the λ_{max}'s of the A_1 and A_2 rhodopsins are sufficiently far apart (~500 nm and ~520 nm, respectively), the contribution of A_2 rhodopsin to sensitivity dominates by a 10:1, or much larger, ratio in the far red. Thus, the error introduced by A_1 rhodopsin to the determination of λ_c for A_2 rhodopsin is very small. Also, λ_{max} of A_2 rhodopsin ranges 521-528 nm in the literature (*16, 18-21*). We found that 523 nm (*19, 21*) fits our data quite well. If 528 nm were used, λ_{max}/λ_c would be 0.84 and 0.85, respectively, from the two methods of deriving λ_c as described in table S1 legend; if 521 nm were used, λ_{max}/λ_c would be the same as the values given in table S1 (0.83 and 0.86, respectively). Thus, the error is very small. For goldfish retina, it has also been reported that perhaps a few percent of the chromophore is A_1 rather than A_2 (*22*). For the same reasons as above – and even more so – this small percentage of A_1 chromophore should not affect the determination of λ_c for goldfish A_2 pigment.

Recordings from mouse rods expressing only mouse S cone pigment. In a transgenic mouse line, the rods co-express both endogenous rhodopsin and the mouse S [ultraviolet (UV)-sensitive] cone opsin (*23*). However, by breeding this line into the rhodopsin knock-out (*rho$^{-/-}$*) genetic background (*24*), the rods express only the S cone pigment (*23*). The rods in the *rho$^{-/-}$* mouse show severe degeneration. The expression of S cone opsin reduces this degeneration, perhaps by restoring some structural integrity to the outer segment, but such rescue is partial and lasts for only about one month after birth (*23*). Accordingly, we recorded from these rods in no later than postnatal 4-5 weeks. That the recordings were indeed from transgenic rods and not native S cones was verified by the characteristic light response (Text Fig. 2C) and the action spectrum. Specifically, the dim-flash response from such transgenic rods had a time-to-peak of 201±45 ms

(mean±SD, n=9), similar to that of wild type rods (217±11 ms) (*25*) and several-fold slower than that of mouse cones (92±7 ms) (*26*). Also, the half-saturating flash intensity was 156±76 photons μm^{-2} at 360 nm (n=4) for these transgenic rods, similar to wild type rods (*25*) and much lower than the S cones (*26*). Finally, these rods showed a single, well-defined λ_{max} in their action spectrum, whereas native mouse cones typically had two λ_{max} peaks because of their co-expression of the M and S cone pigments (*26*).

Determination of E_a^P without the extrapolation method. Following previous work (*12, 27-29*), instead of the extrapolation method to determine λ_c and therefore E_a^P (= hc/λ_c), a direct way to evaluate E_a^P, albeit less intuitive, is to start with the general expression:

$$S \propto \exp[-hc/kT(1/\lambda_c - 1/\lambda)] \times \sum_1^m [1/(m-1)!](hc/kT)^{m-1}(1/\lambda_c - 1/\lambda)^{m-1} \qquad (S1)$$

which can be derived from Text Eq. 1 (but replacing E_a^T with hc/λ_c - hc/λ). Here, S is spectral sensitivity, h is Planck's constant, c is speed of light, k is Boltzmann's constant, and m is the number of vibrational modes in the pigment molecule that contribute thermal energy to photoisomerization. From eq. S1, it can be shown (*27*) that E_a^P is given by:

$$E_a^P = hc/\lambda_c = hc/\lambda + (hc/T)\{-[\partial\log_{10}S/\partial(1/T)]/[\partial\log_{10}S/\partial(1/\lambda)]\} \qquad (S2)$$

where the partial derivatives represent, respectively, the rate of change in $\log_{10}S$ with respect to $1/T$ at a given λ and the rate of change in $\log_{10}S$ with respect to $1/\lambda$ at a given T. Thus, E_a^P can be evaluated without explicitly knowing m. We carried out calculations according to Koskelainen *et al.* (*28*), as follows. At each long wavelength (λ_i) where experimental measurements were made, we calculated -$[\partial\log_{10}S/\partial(1/T)]$ as $[\log_{10}S_{i,W} - \log_{10}S_{i,C}]/[(1/T_C - 1/T_W)]$, and $[\partial\log_{10}S/\partial(1/\lambda)]$ as the mean of $[\log_{10}S_{i-1,C} - \log_{10}S_{i,C}]/(1/\lambda_{i-1} - 1/\lambda_i)$ and $[\log_{10}S_{i,C} - \log_{10}S_{i+1,C}]/(1/\lambda_i - 1/\lambda_{i+1})$, where the subscripts i-1, i and i+1 represent parameter values at λ_{i-1}, λ_i and λ_{i+1}, and the subscripts W and C represent "warm" and "cold" temperatures, respectively. We also set $T = T_C$ in eq. S2. The E_a^P values obtained at different λ_i were very similar (not shown), and were averaged to give the E_a^P for a given cell. Table S1, second rightmost column, shows the overall average of E_a^P for each photoreceptor type studied. From E_a^P, λ_c can be calculated, and therefore λ_{max}/λ_c from the known λ_{max} (table S1, rightmost column). Although Text Fig. 4A and fig. S9 indicate that m actually varies with λ, the m variation, over the short range of descent (3 log units) of the spectrum at long wavelengths used in the above calculations, is nonetheless minimal, and presumably unimportant.

Multi–vibrational-mode thermal statistics (Text Eq. 1). We used Text Eq. 1 as a heuristic approach that is simple and applicable across rod and cone pigments. It is also the realistic approach at present, for several reasons. First, molecular-dynamics computations would involve model-dependent parameters (e.g., *30*). Even for rhodopsin, however, many molecular details from spectroscopy for photoexcitation are not necessarily applicable to thermal excitation (see Main Text). Second, although the solved crystal structure of rhodopsin (*31*) has greatly facilitated molecular computations on this pigment (e.g., *32-37*), a comprehensive pigment-noise theory, such as that developed here, should include cone pigments, for which little structural information is available. Third, despite its indisputable occurrence, spontaneous activation is an exceedingly rare molecular event (i.e., happens with exceedingly low probability). For example, rhodopsin has a thermal-activation time constant (i.e., reciprocal of rate constant) of ~1,000 years. Molecular-dynamics calculations on this time scale would be currently challenging (*30*). Fourth, there is the recent suggestion that rhodopsin may be dimeric (*38*), thus further complicating the

calculations. Finally, quantum-mechanics/molecular-dynamics calculations appear to lack the precision we need. As an example, various calculations of this kind (*32,35,37,39*) have arrived at bathorhodopsin energetically being only at 7.3-26 kcal mol^{-1} above dark rhodopsin – quite variable and all drastically lower than the accepted measured value of ~35 kcal mol^{-1} [(*40*), but see (*41*)]. By contrast, our approach needs only two parameters: the ground-state isomerization energy barrier, E_a^T, and the number of vibrational modes, *m*, contributing energy to the reaction. Both parameters can be specified from our experimental measurements. Although our simple theory does not provide a detailed molecular description of the thermal-activation process, it can serve as a framework upon which molecular details can be added in the future.

Derivation of the number of vibrational modes, *m*, for thermal isomerization. In different publications involving Text Eq. 1, the notation for the number of vibrational modes has varied, although the physical meaning is the same. In Hinshelwood's monograph (*42*), the parameter *n* denotes the total number of "quadratic energy terms" (= potential energy + kinetic energy) in the vibrational modes (our parameter *m*). With each vibrational mode having two quadratic energy terms, we have $m = n/2$. St. George (*8*) used the same notation as Hinshelwood, calling *n* the degrees of freedom. Lewis (*5*) adopted *m* as $m = (n/2) - 1$, and defined the number of vibrational modes as *m*+1. Srebro and Behbehani (*9*) redefined *m* as the number of vibrational modes, i.e., $m = n/2$. Finally, Ala-Laurila *et al.* (*43*) followed Lewis' notation. In the present paper, we chose to follow Srebro and Behbehani's notation because it seems to be more intuitive. In particular, we like the fact that, when $m = 1$, Text Eq. 1 reduces to the Boltzmann distribution. In our notation, a non-linear molecule such as 11-*cis*-retinal with *N* atoms has a maximum *m* value of $3N - 6$ (*44*).

The *m* value for thermal isomerization of rhodopsin can be obtained from the relation $E_a^T - E_a^{T(app)} = (m-1)RT$, which is derived from Text Eq. 1 by using only the first term in the summation series as an approximation and is valid for $E >> RT$ (*8, 42*). The *m* value of 45 at 23°C that we obtained in this way is higher than the *m* value of 40 previously obtained by Ala-Laurila et al. (*43*) based on their measured (*12*) E_a^P of 44.3 kcal mol^{-1} and the assumption of $E_a^T = E_a^P$ for *Bufo* rhodopsin. If the above approximation were not used, *m* would have to be obtained by trial and error from the requirement of giving an $E_a^{T(app)}$ value of exactly 21.9 kcal mol^{-1} (*45*). With our parameters, this would have yielded *m* ~46, still very similar to 45. This is about one third of the total number of vibrational modes available in the chromophore itself of visual pigments (141 in total, contributed by the 49 atoms in the chromophore molecule), although some of the contributing modes could potentially have come from the opsin as well.

Measurement of thermal activity in *Bufo* red rod. Although the thermal activity in *Bufo* red rods has been measured 30 years ago (*45*), we repeated the measurements in this study for uniformity in measurements and data analysis. After positively identifying the red rods, 60 identical dim flashes were delivered (see sample in fig. S3A, upper panel). Variance analysis on the response ensemble gave a single-photon–response amplitude of about 1 pA. Subsequently, ten minutes of continuous dark recording were made (fig. S3A, lower panel), from which the thermal-event rate was estimated based on three methods (*46*). The first was to simply identify and count the quantal events based on a criterion amplitude being at >30% of the single-photon–response amplitude and a criterion integration time being within 50-200% of the average dim-flash response (*46*). From 4 cells, the rate was 0.024 ± 0.003 s^{-1} (SD). The other two methods

were more objective. In the probability-density method (*46*) (fig. S3B), a probability-density histogram was computed from the 10-min dark recordings. This histogram was almost symmetrical about 0 pA, except for some excess probability in the 0.4-1.6 pA range reflecting the presence of the discrete events in darkness. As confirmation, selected segments within the 10-min recording with no obvious discrete events gave a symmetrical probability-density histogram (red profile in fig. S3B). From the same 4 cells as above, we estimated from the excess probability density a dark-event rate of 0.032 ± 0.014 s^{-1}. Finally, in the power-spectrum method (*46*), we computed the power-density spectra from selected segments (within the same 10-min recording) with discrete events and those without obvious events, respectively. By fitting the square of the Fourier transform of the single-photon–response profile (fig. S3C inset) to the difference spectrum (i.e., the difference between the two power spectra with and without events; fig. S3C), we obtained 0.020 ± 0.006 s^{-1} from the 4 cells. The values from all three methods are quite similar, with a mean of 0.025 s^{-1}. Dividing this rate by the pigment content in the recorded part of the cell (table S5) gave a rate constant of 4.18×10^{-12} s^{-1}, a factor of 2 lower than the previous measurement of 1×10^{-11} s^{-1} at ~20°C (*45*). The actual difference is smaller because the previous measurement (*45*) made use of a pigment density that was somewhat lower than the 3.5 mM adopted in the present paper (see table S5 legend). The remaining difference reflects a certain margin of error due to the rod's "continuous noise" originating from downstream of the pigment (*45*), which may confound the detection of the discrete events. Thus, the discrepancy between the two measurements should be considered acceptable.

Extrapolation of noise rate to 23°C for A$_1$ human red cone pigment and mouse rhodopsin. We used mice with a *GCAPs$^{-/-}$* genetic background (in order to boost the single-photon–response amplitude, and hence the thermal-event size, to a detectable level), and with or without human red cone pigment expressed transgenically in their rods (i.e., *GCAPs$^{-/-}$* versus *OPN1LW^{+} GCAPs$^{-/-}$*) (*46*). Lowering temperature from 37°C (*46*) to 29°C (data collected in this study) substantially reduced the thermal events in the rods from both lines (fig. S4A, B). For 37°C, multiple methods were used for counting events (*46*) (see also **Measurement of thermal activity in *Bufo* red rod** above), giving a similar rate as previously reported (*47*); for 29°C, however, only the visual-counting method was used. From *GCAPs$^{-/-}$* rods, we obtained the thermal rate for rhodopsin at each temperature, and likewise from *OPN1LW^{+} GCAPs$^{-/-}$* rods the combined rate of both pigments. From the difference between *GCAPs$^{-/-}$* rods and *OPN1LW^{+} GCAPs$^{-/-}$* rods, we obtained the rate for red cone pigment at each temperature. Dividing these rates by the respective pigment contents (table S5), we obtained the rate constants. The temperature dependences of the rate constants for both pigments are shown in the Arrhenius plot of fig. S4C (logarithmic rate constant against reciprocal absolute temperature). By linear extrapolation, we obtained the rate constant of each pigment at 23°C, which is otherwise immeasurable because the dark current would be too small at 23°C and the dark events therefore unresolvable. A linear relation between logarithmic rate constant and reciprocal temperature is obvious from the Arrhenius equation (or Boltzmann's distribution), but we found this to be also approximately true for multi–vibrational-mode thermal statistics (i.e., Text Eq. 1), at least in the limited temperature range under consideration (fig. S5). From the left plot in fig. S4C, the apparent thermal activation energy for A$_1$ rhodopsin, $E_a^{T(app)}$, is 14.54 kcal mol^{-1}, versus an expected 22.16 kcal mol^{-1} [from E_a^T - $E_a^{T(app)}$ = $(m-1)RT$, or $48.03 - (45-1) \times 0.588$ kcal mol^{-1} = 22.16 kcal mol^{-1}] based on a λ_{max} of 500 nm, or the previous estimate of 21.9 kcal mol^{-1} for *Bufo* rhodopsin (*45*). From the right plot in fig. S4C, $E_a^{T(app)}$ for A$_1$ red cone pigment was 14.64 kcal mol^{-1}, versus an

expected 17.25 kcal mol^{-1} [from $43.12 - (45-1) \times 0.588$ kcal mol^{-1} = 17.25 kcal mol^{-1}] based on a λ_{max} of 557 nm. These discrepancies reflect a margin of error in the measured rates of thermal events. Thus, the extrapolated values at 23°C are only approximate.

Immunocytochemical labeling of blue cone pigment in *Bufo* green rods. Like other amphibians, the toad, *Bufo marinus*, has two types of rods: red rods and green rods, with red rods being the majority. In many amphibians, green rods have been found to express the blue cone pigment as do blue cones (*48-50*). We checked with immunocytochemical labeling whether *Bufo* green rods also express the blue cone pigment.

An intact toad eye was fixed with 4% paraformaldehyde in PBS for 1 hr at room temperature, then washed 3 times with phosphate buffer saline (PBS). The fixed eyes were equilibrated with 30% sucrose in PBS overnight. After removal of the cornea and the lens, four cuts were made radially towards the center of the eyecup, and the latter was then flattened and embedded in OCT (Tissue-Tek). Afterwards, 14-μm sections were cut on the cryostat. The sections were washed three times with PBS, blocked in blocking buffer (5% normal goat serum in PBS with 0.3% Triton X-100) for 1 hr, and incubated overnight with primary antibodies in blocking solution at 4°C: 4D2 monoclonal antibody against rhodopsin (*51*) (1:50 dilution) and Blue-N polyclonal antibody against blue cone pigment (*49*) (1:500 dilution). The 4D2 antibody was raised in mouse against the N-terminus of bovine rhodopsin, but has been shown to recognize rhodopsin in frog and salamander red rods (*51, 52*). The Blue-N antibody was raised in rabbit against the N-terminus of salamander blue-sensitive cone opsin, and is known to label green rods in salamander (*49*) and *Xenopus* (J.-X. Ma, personal communication). On the following day, the sections were washed five times in wash buffer (PBS with 0.3% Triton X-100) for 5 min each, and incubated with secondary antibodies: Alexa Fluor 647-conjugated goat anti-mouse IgG (1:500 dilution, Molecular Probes) and Alexa Fluor 488-conjugated goat anti-rabbit IgG (1:500 dilution, Invitrogen). Finally, the sections were washed five times in wash buffer, mounted with Fluoromount-G (Electron Microscopy Sciences) and overlaid with coverslips.

Confocal images showed morphologically distinct blue-cone-pigment-positive photoreceptors and rhodopsin-positive photoreceptors (fig. S6A). The former had outer and inner segments characteristic of *Bufo* green rods (see below). Thus, *Bufo* green rods indeed express a blue cone pigment.

Measurement of thermal activity in *Bufo* green rods (i.e., blue cone pigment). In *Bufo marinus*, the red and green rods can be differentiated based on their distinct morphology and spectral sensitivity. The outer segment of both rod types has a diameter of 5-8 μm, but is typically longer for red rods (up to 80 μm) than for green rods (up to 60 μm). The inner segment is more distinct between them, being $\leq$ 10 μm long for red rods, and up to tens of microns long but rapidly tapering to 1 μm in diameter for green rods (fig. S6B, left panels). However, some red rods do have shorter outer segments and can resemble green rods, especially if the narrow part of the inner segment is truncated and the soma is lost during dissociation. Their identities can nonetheless be confirmed by the action spectrum, because λ_{max} is 432 nm for green rods (fig. S7) (*53*) and 500 nm for red rods. Therefore, at approximately the same photon intensity, a 440-nm flash elicits a larger response from a green rod than a 500-nm flash, and the opposite is true for a red rod (fig. S6B, middle panels). Finally, the dark current is generally much larger for the

red rod than the green rod (fig. S6B, right panels). For thermal-noise experiments, we accepted only dark currents greater than 10 pA for the green rods in order that the unitary events were readily identifiable (see Text Fig. 3).

In the dim-flash experiment in Text Fig. 3A-C, the curve fitted to the response-amplitude histogram in panel C is drawn with the Poisson distribution blurred by Gaussian functions (*54*):

$$p(r) = \sum_{q=0}^{\infty} \frac{e^{-s} s^q}{q!} \frac{1}{\left(2\pi\left(\sigma_0^2 + q\sigma_1^2\right)\right)^{\frac{1}{2}}} \exp\left(-\frac{(r - qa)^2}{2\left(\sigma_0^2 + q\sigma_1^2\right)}\right) \tag{S3}$$

with s=0.33, a=1.1 pA, σ_0=0.09 pA, σ_1=0.12 pA. Here, $p(r)$ is the probability of the response amplitude being r pA, a is the mean single-photon–response amplitude, σ_0^2 is the variance of the baseline noise in darkness, σ_1^2 is the variance of the single-photon response, and s is the mean number of unitary responses elicited per flash trial.

The thermal-activation events of the blue cone pigment in *Bufo* green rods (23°C) were well resolved by visual inspection, without the need to resort to probability-density and power-spectrum calculations. Indeed, the events were so rare that the latter methods would not have been useful. Also, such a low event rate was impossible to be estimated from any one cell. Instead, we collected 10-minute recordings epochs from cells – some cells providing just one epoch and others providing more – and combined them for calculations, as follows. Suppose the average rate of thermal activity is v. The mean number of events for an epoch of constant duration T is thus vT. For a Poisson stream, the probability of no event (p_0), one event (p_1), two events (p_2), etc. in an epoch is given by $p_0 = e^{-vT}$, $p_1 = vT\,e^{-vT}$, $p_2 = [(vT)^2/2]\,e^{-vT}$, etc. In the experiment of Text Fig. 3I, there were altogether 83 epochs, of which 69 had no events, 13 had one event, and 1 had two events. Fitting the Poisson prediction with $T = 10$ min and different v values to these measurements gave $v = 0.00031$ s^{-1}, which is remarkably close to the grand mean obtained from $15/(83 \times 10 \times 60$ s$) = 0.00030$ s^{-1}. Dividing by the pigment content (table S5) gave the rate constant.

Prediction of long-wavelength descent of absorption/action spectral template. In Text Fig. 4A and B, the spectral templates were all plotted according to the following equation:

$$S(\lambda) = \frac{1}{\exp\left[69.7 \times \left(0.88 - \frac{\lambda_{max}}{\lambda}\right)\right] + \exp\left[28 \times \left(0.922 - \frac{\lambda_{max}}{\lambda}\right)\right] + \exp\left[-14.9 \times \left(1.104 - \frac{\lambda_{max}}{\lambda}\right)\right] + 0.674} \tag{S4}$$

based on Eq. 1 in Govardovskii *et al.* (*55*), which is modified from Lamb's equation (*6*). This equation is an empirical fit to collected spectra from various amphibian, fish and reptile A$_1$ rod and cone pigments at presumably room temperature (not specified by the authors). For the purpose of Text Fig. 4A and B, we assume the template to hold reasonably well at 23°C. Incidentally, the form of eq. S4 predicts that all spectral templates, when plotted as logarithmic sensitivity against λ_{max}/λ, will superpose exactly (as shown in Text Fig. 1B, inset), and that, when plotted against $1/\lambda$, they will all converge at $\lambda \rightarrow \infty$.

For predictions of the descent of the spectrum at $\lambda > \lambda_c$, we start with:

$$f_{\geq E} = e^{-\frac{E}{RT}} \sum_{1}^{m} \frac{1}{(m-1)!}\left(\frac{E}{RT}\right)^{m-1}$$

(S5)

which is essentially Text Eq. 1 but with a general energy E as the parameter. Here, $f_{\geq E}$ is the fraction of molecules with contributing thermal energy (from m vibrational modes) equal to or greater than a criterion energy E in kcal mol^{-1}. The thermal energy, ΔE, required for supplementing the photon energy at λ in order to reach the photoactivation energy, E_a^P, is given by $\Delta E = E_a^P - hc/\lambda$. Replacing E_a^P by hc/λ_c, we have $\Delta E = hc[1/\lambda_c - 1/\lambda]$. Substituting ΔE for E in eq. S5, we have:

$$f_{\geq \Delta E} = \exp\left[-\frac{hc}{RT}\left(\frac{1}{\lambda_c} - \frac{1}{\lambda}\right)\right] \times \sum_{1}^{m} \frac{1}{(m-1)!}\left[\frac{hc}{RT}\left(\frac{1}{\lambda_c} - \frac{1}{\lambda}\right)\right]^{m-1}$$

(S6)

With photosensitivity, S, being proportional to $f_{\geq \Delta E}$, or $S = rf_{\geq \Delta E}$, where r is a constant, we have:

$$\log_{10} S = \log_{10} r - \frac{hc}{RT}\left(\frac{1}{\lambda_c} - \frac{1}{\lambda}\right) \times \log_{10} e + \log_{10} \sum_{1}^{m} \frac{1}{(m-1)!}\left[\frac{hc}{RT}\left(\frac{1}{\lambda_c} - \frac{1}{\lambda}\right)\right]^{m-1}$$

(S7)

The prediction from eq. S7 (at 23°C) is shifted vertically to match a spectral template (with given λ_{max}) at λ_c (= $\lambda_{max}/0.84$) by adjusting r in eq. S7. In Text Fig. 4A, the dashed curves are eq. S7 with $m = 1, 2, 3$ etc. In Text Fig. 4B, the two dashed curves (one barely visible because it coincides with the long-wavelength descent of the template with $\lambda_{max} = 698$ nm) are eq. S7 with $m = 1$.

In Text Fig. 4B, the λ_{max} of 698 nm, chosen so that the long-wavelength descent of its spectral template matches eq. S7 with $m = 1$ throughout, is calculated in the following way. For $m = 1$, eq. S7 reduces to:

$$\log_{10} S = \log_{10} r - \frac{hc}{RT}\left(\frac{1}{\lambda_c} - \frac{1}{\lambda}\right) \times \log_{10} e$$

(S8)

which has a slope of $(hc/RT) \times \log_{10} e$ when $\log_{10} S$ is plotted against $1/\lambda$. The slope of the long-wavelength descent in the spectral template above (eq. S4) when plotted as $\log_{10} S$ against λ_{max}/λ is evaluated to be 30.27 [see also (3, 6)], or $30.27 \times \lambda_{max}$ when plotted against $1/\lambda$. Thus, from $(hc/RT) \times \log_{10} e = 30.27 \times \lambda_{max}$, we obtain $\lambda_{max} = 698$ nm at 23°C.

Values of constants. For all calculations, we have adopted $h = 6.62607 \times 10^{-34}$ Joule s, $c = 299{,}792{,}458$ m s^{-1}, $R = 1.9858775$ cal K^{-1} mol^{-1}, $N_A = 6.02214 \times 10^{23}$, 1 cal = 4.184 Joule, and [K] = [°C] + 273.15.
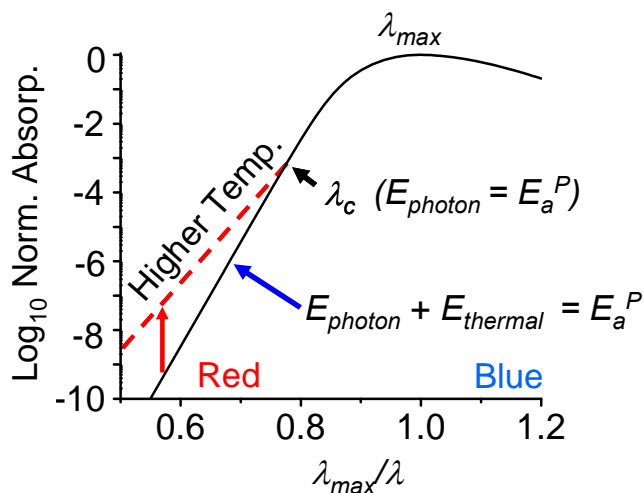
Fig. S1. Schematic diagram showing the temperature effect on photoisomerization. A spectral template is plotted as logarithmic normalized absorption against reciprocal normalized wavelength (λ_{max}/λ). At a higher temperature, absorption at the long-wavelength part increases, as shown exaggerated by the red dashed line, because of a higher percentage of pigment molecules having sufficient complementary thermal energy ($E_{thermal}$) for photoisomerization. The red and black spectra intersect at the critical wavelength, λ_c, with photon energy (E_{photon}) exactly equal to the minimal photoactivation energy, E_a^P. At wavelengths shorter than λ_c, the photon has energy already higher than E_a^P; thus no thermal energy is required, and the absorption shows no temperature-dependence. "Red" and "Blue" indicate longer and shorter wavelengths, respectively.
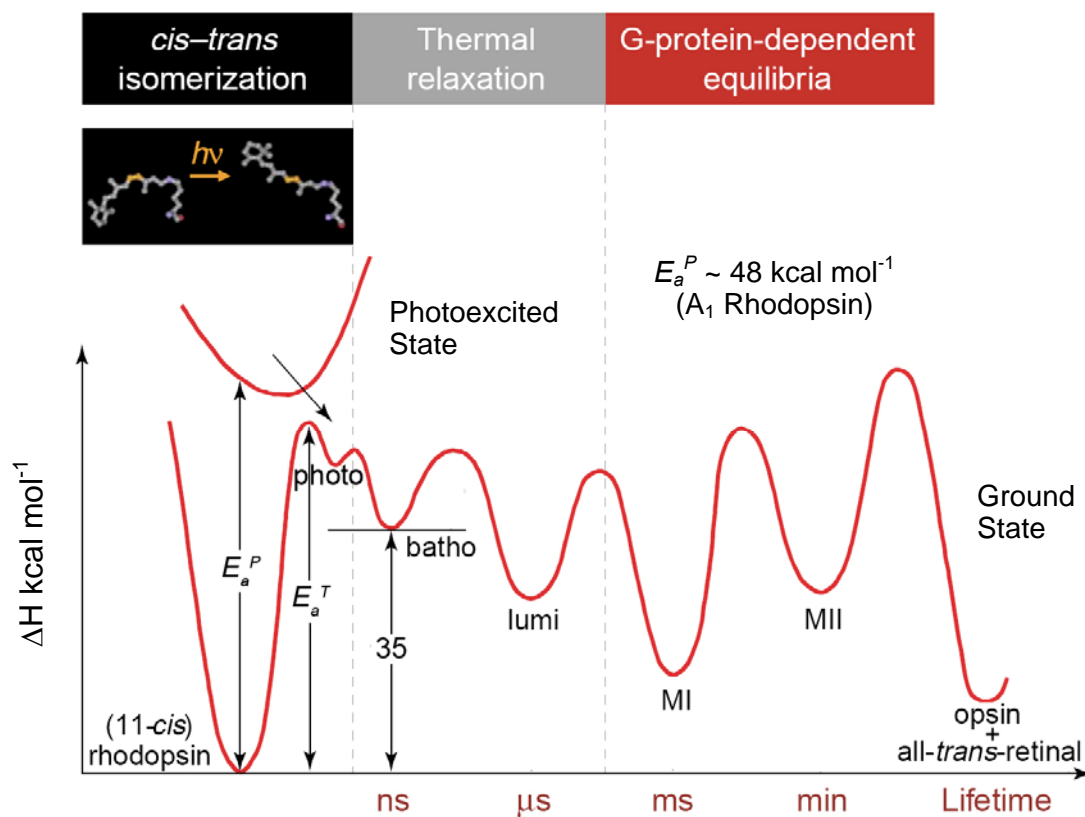
Fig. S2. Energy diagram for activation of rhodopsin, modified from Fig.5a in Okada *et al.* (*56*). A photon is absorbed only when its energy (or when its energy in combination with rhodopsin's thermal energy) is sufficient for reaching the minimum photoactivation energy, E_a^P (~48 kcal mol^{-1}, see table S1). Rhodopsin transits very rapidly to the photoexcited state. Within 200 fs or less (*57, 58*), it relaxes back to the ground state and at the same time crosses the ground-state isomerization energy barrier, E_a^T, with a quantum efficiency of 0.67, leading to the formation of photorhodopsin. It then thermally decays through the intermediate photoproducts of batho, lumi, MI to the active state, MII, which triggers phototransduction via a G-protein signaling cascade. Finally, MII decays into free opsin and all-*trans*-retinal. Bathorhodopsin has been shown to store up to 35 kcal mol^{-1} of the absorbed photon energy (*40*).
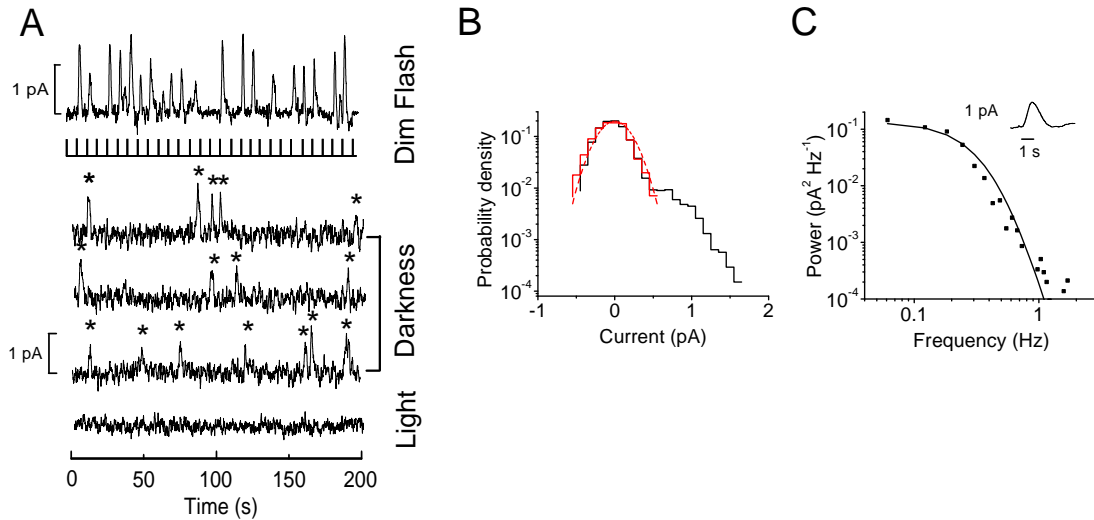
Fig. S3. Thermal activity in a *Bufo* red rod at 23°C. **(A)** Top trace, sample responses to identical dim flashes delivered repetitively at timings indicated by vertical bars. The average flash intensity was low enough to elicit no response or a clearly discernible single-photon response in some trials. Middle three traces, 10-min continuous recording from the same cell in darkness displayed in three 200-s segments. Single-photon-response–like events are marked by stars. Bottom trace, recording under continuous saturating light, to indicate the non–transduction-related background noise. Recordings were low-pass filtered at 3 Hz. **(B)** Probability-density histogram (black) of overall dark recordings in A. Bin-width is 0.1 pA. Red histogram is that of selected recording segments without any obvious events, and is scaled to the same height as the overall dark recording; it is well fit by a Gaussian function (red dashed curve). **(C)** Difference power-density spectrum of the same dark recordings in **(A)** (power spectrum with events minus power spectrum without events, both in darkness), fit by a power spectrum computed from the single-photon response (inset) with a scaling factor corresponding to the event frequency. Dividing this frequency by the appropriate pigment content (table S5) gave the rate constant.
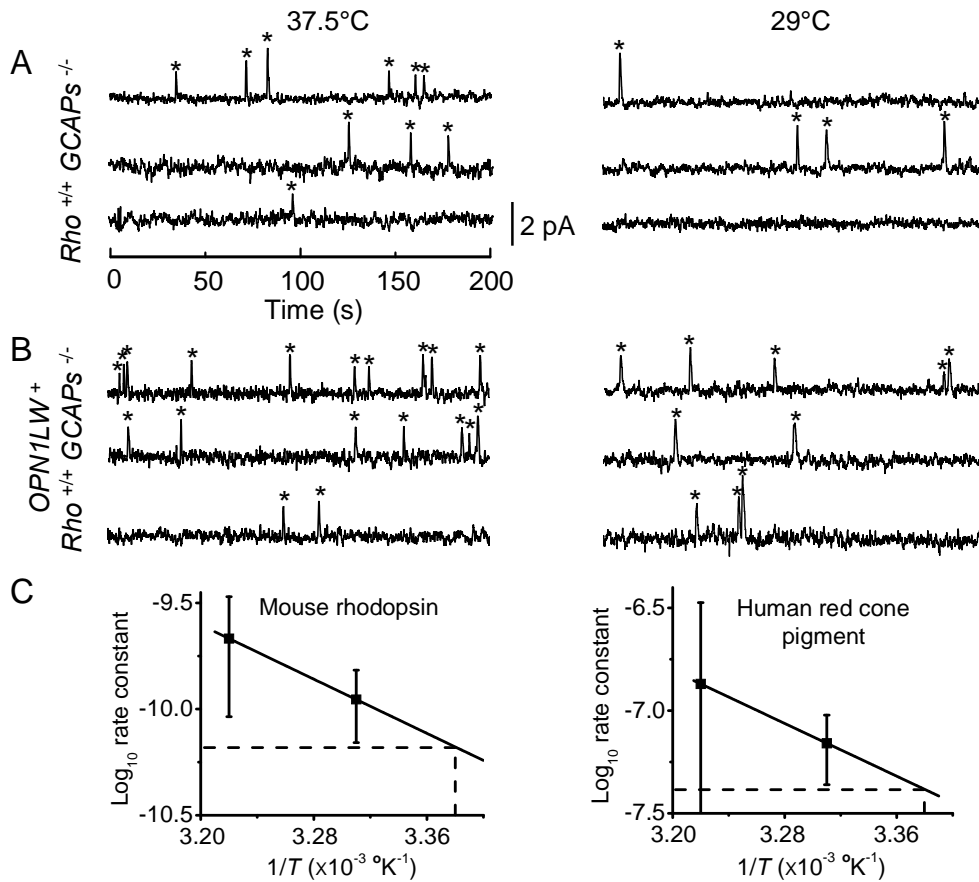
Fig. S4. Effect of temperature on thermal activity of mouse rhodopsin and human red cone pigment. Recordings were made from *GCAPs*^{-/-} mouse rods with or without transgenically expressed human red cone pigment, and low-pass filtered at 3 Hz. The *GCAPs*^{-/-} background removes some strong negative feedback on phototransduction, thus increasing the single-photon response by several-fold and allowing identification of the thermal events (marked by stars). **(A)** Thermal events of rhodopsin recorded from a *Rho*^{+/+} *GCAPs*^{-/-} rod in darkness at 37.5°C [data from (*46*)] and at 29°C (this study). **(B)** A higher rate of thermal events recorded from a *OPN1LW*^{+} *Rho*^{+/+} *GCAPs*^{-/-} rod, which also expresses transgenic human red cone pigment, at 37.5°C (*46*) and at 29°C (this study). The difference between the two rates at each temperature gave the thermal rate for red cone pigment. Dividing the rates by the appropriate pigment contents (table S5) gave the rate constants. **(C)** Logarithmic rate constant plotted against reciprocal temperature for each pigment. Linear extrapolation gave estimates at 23°C (=296 K).

13
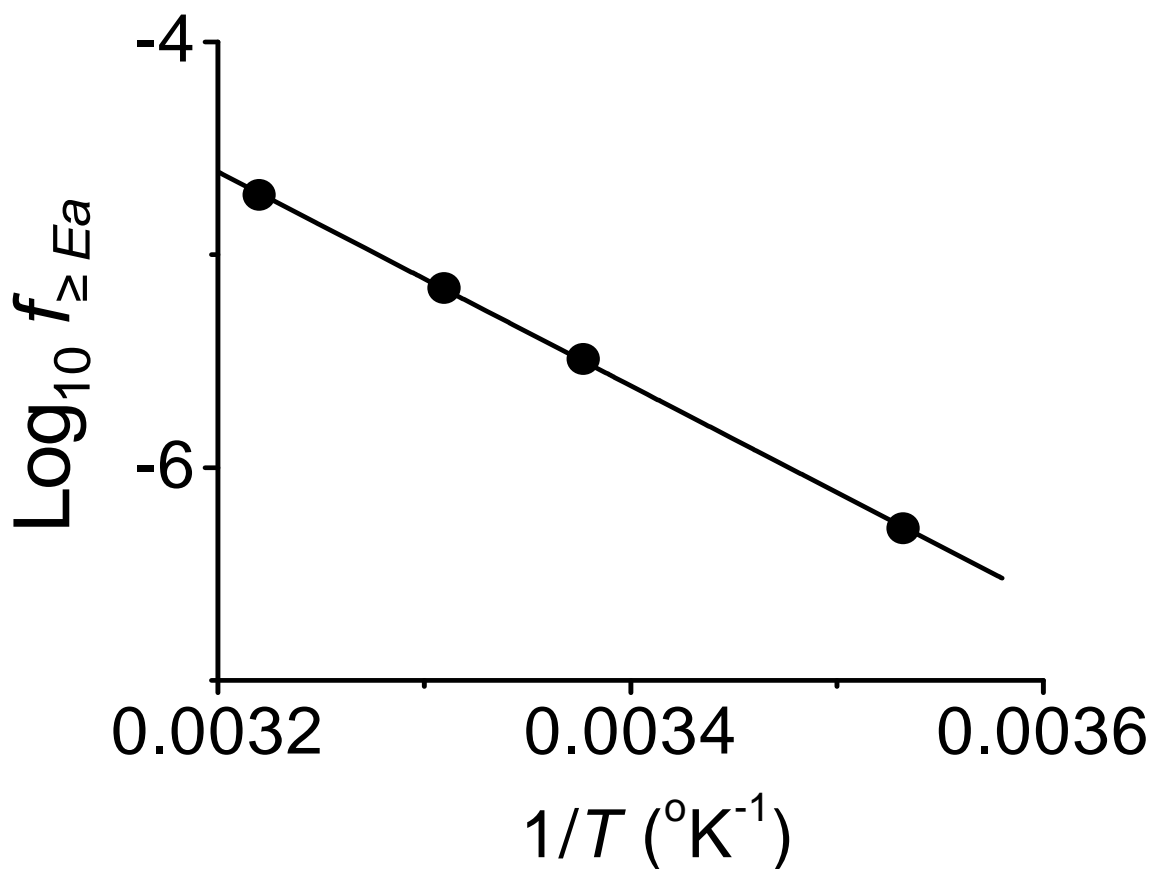
Fig. S5. Arrhenius plot showing a quite-linear relation between logarithmic $f_{\geq Ea}$ (and hence thermal-activity rate constant) and reciprocal absolute temperature. To justify the use of linear extrapolation in fig. S4 for obtaining the thermal-activity rate constant at 23°C, we need to confirm that the multi–vibrational-mode thermal statistics (i.e., Text Eq. 1) can be approximated by a linear fit, as demonstrated at least over the temperature range here, by using as an example $E_a^T = 48.03$ kcal mol^{-1}, $m = 45$, and $T = 37.5, 29, 23$ and 10°C.
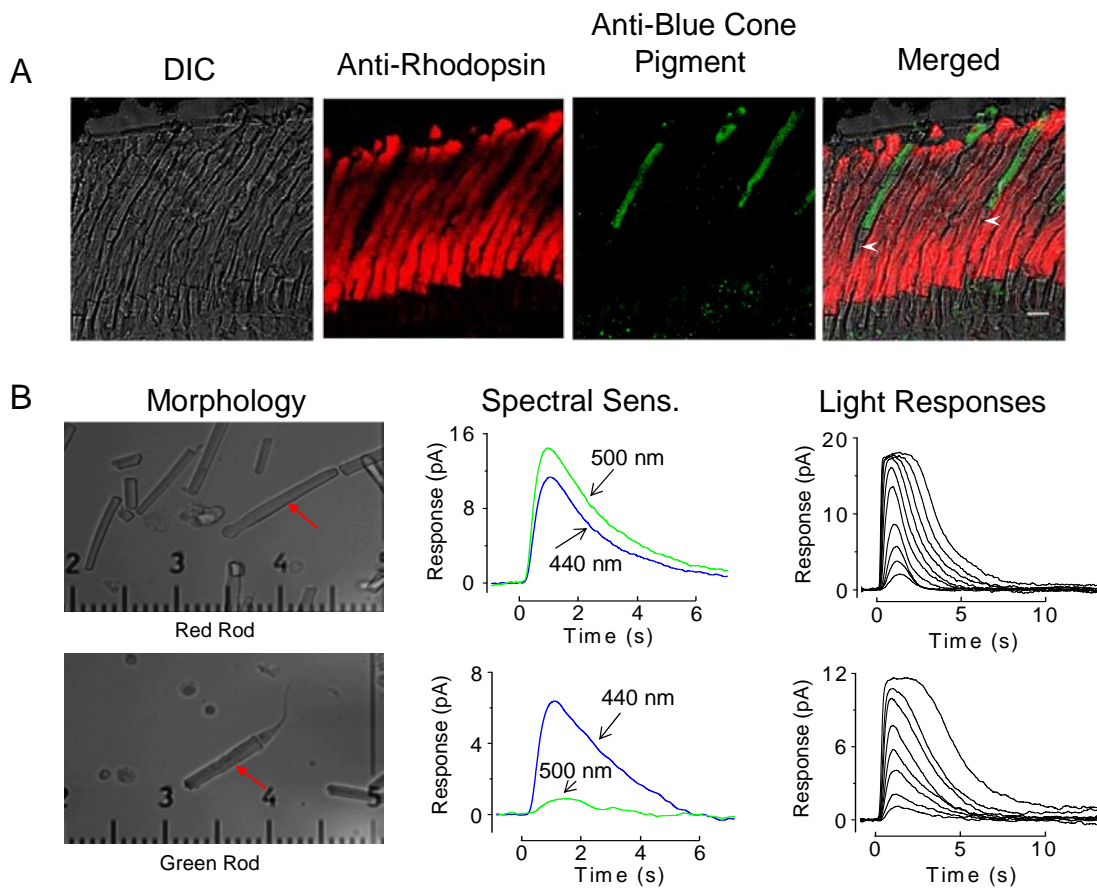
Fig. S6. Differences between *Bufo* red and green rods. **(A)** Immunocytochemistry of *Bufo* retinal section showing rhodopsin in red rods and blue cone pigment in green rods. Confocal microscopy for right three images. Antibody 4D2 (*51*) against rhodopsin and Blue-N (*49*) against blue cone pigment. Arrow heads indicate tapered inner segments typical of the green rods. Scale bar is 10 μm. **(B)** Left panels, morphology of red and green rods. Red arrows mark an example of each. See **Materials and Methods** for details. Each small division in the scale is about 6 μm. Middle panels, flash responses showing different spectral sensitivities of red and green rods. 500-nm and 440-nm flashes at the same sub-saturating intensity of 2.3 photons μm^{-2} elicited different response amplitudes from the two rod types. Right panels, responses elicited from each rod type by flashes of increasing intensity (by successive factors of roughly 2).
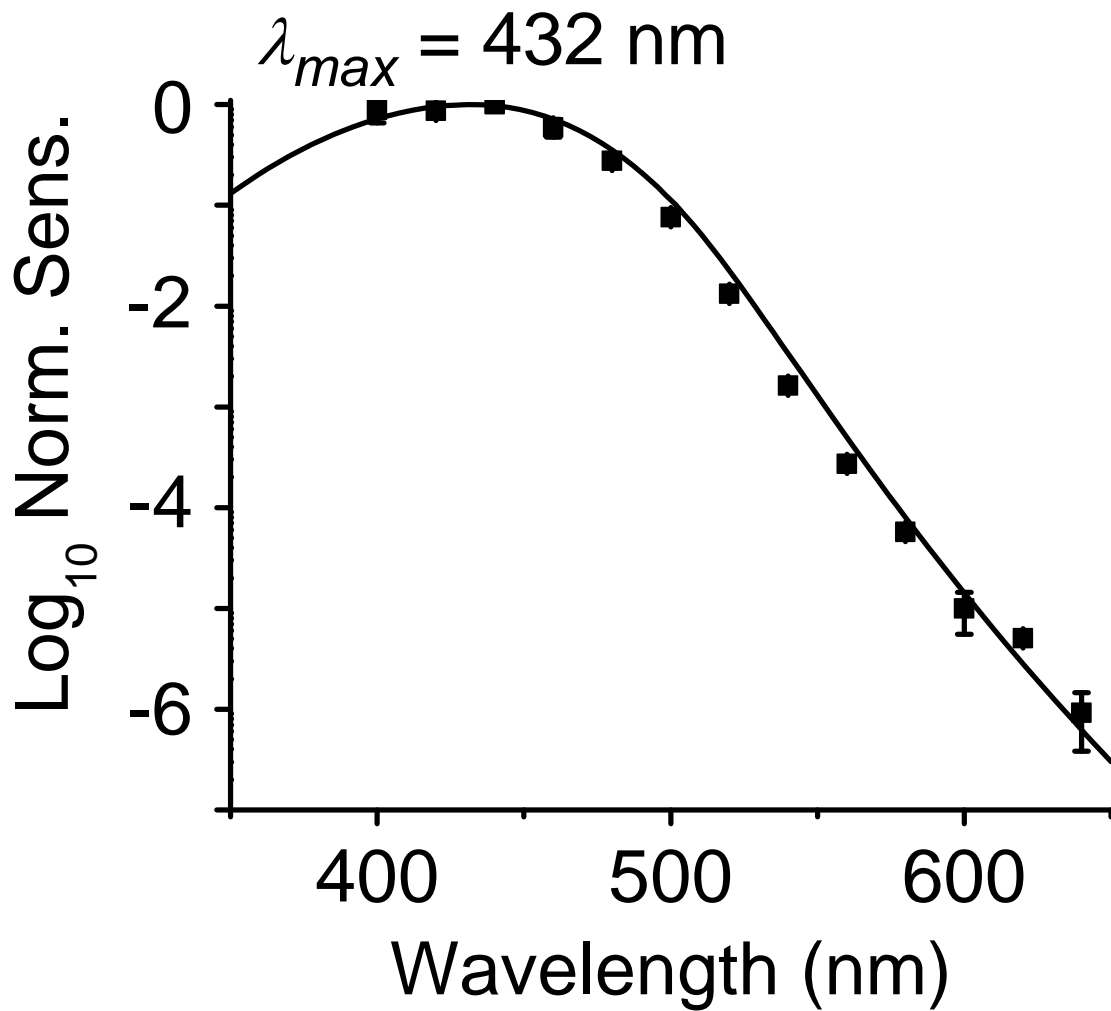
Fig. S7. Action spectrum of *Bufo* green rods. Error bar is SEM. The solid curve is a fit with an A_1 pigment spectral template (*55*) with a λ_{max} of 432 nm.
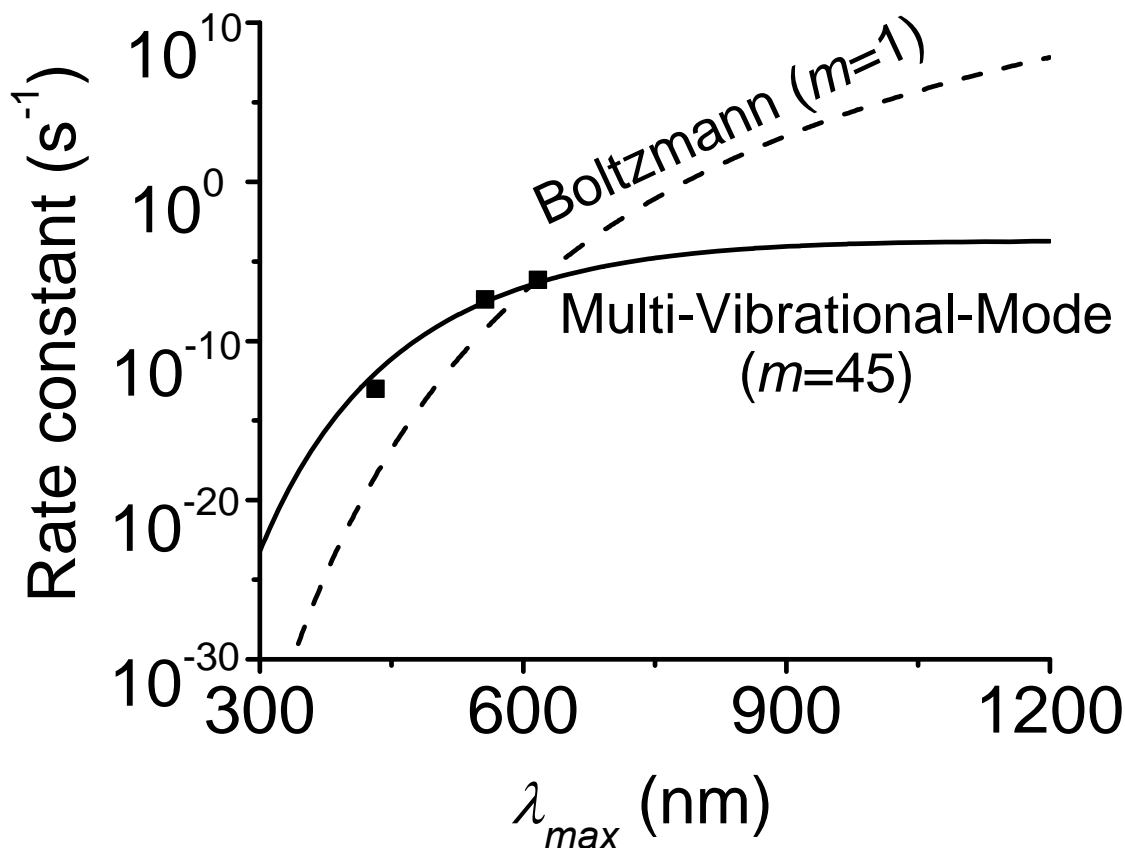
Fig. S8. Multi–vibrational-mode thermal statistics, but not Boltzmann statistics, correctly predicts pigment noise. Measured pigment-noise rate constant in log scale is plotted against λ_{max}. Black squares show experimental data from *Bufo* blue cone pigment (with A_1 chromophore) and human red cone pigment with A_1 and A_2 chormophore, respectively (cf. Text Fig. 4C). Solid curve is drawn from $A \times f_{\geq E_a^T}$ (where $f_{\geq E_a^T}$ is given by Text Eq. 1) at 23°C, with $E_a^T = 0.84 hc/\lambda_{max}$,

$m = 45$ and $A = 1.88 \times 10^{-4}$ s^{-1}. Dashed curve is drawn from Boltzmann's distribution, $A \times e^{-\frac{E_a^T}{RT}}$ (i.e., $f_{\geq E_a^T}$ with $m = 1$) at 23°C, with also $E_a^T = 0.84 hc/\lambda_{max}$, but $A = 3.80 \times 10^{22}$ s^{-1}, so chosen in order to make the curve arbitrarily coincide with measurement at λ_{max} of 617 nm. It is clear that Boltzmann's distribution deviates radically from the measurements in terms of the dependence of the rate constant on λ_{max}.
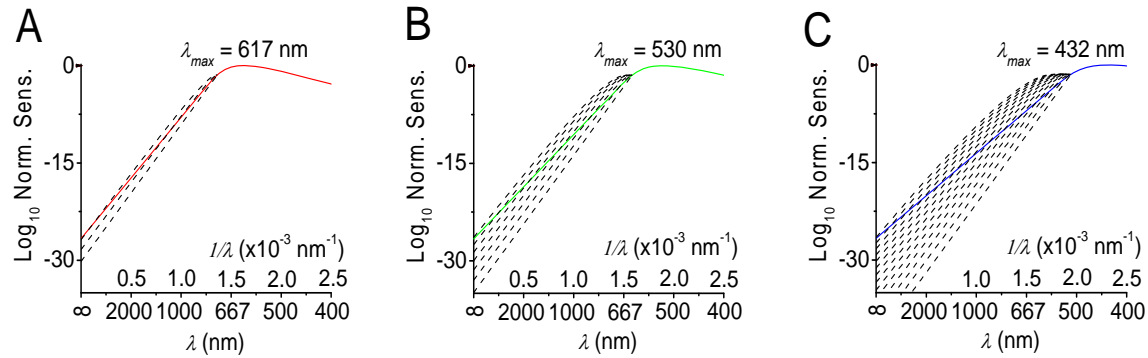
Fig. S9 Comparison between cone pigment templates and predicted descent at wavelengths longer than λ_c. **(A)** Solid red curve is the spectral template for A_2 red cone pigment with λ_{max} =620 nm. Dashed curves are drawn from eq. S7 with m = 1 through 4. For a 10-log unit descent from peak, the requisite m is <3. **(B)** Solid green curve is the spectral template for A_1 green cone pigment with λ_{max} =530 nm. Dashed curves are drawn from eq. S7 with m = 1 through 7. For a 10-log unit descent from peak, the requisite m is <4. **(C)** Solid blue curve is the spectral template for A_1 blue cone pigment with λ_{max} =433 nm. Dashed curves are drawn from eq. S7 with m = 1 through 14. For a 10-log unit descent from peak, the requisite m is <6.

Table S1. Minimum photoactivation energy, E_a^P, and its associated λ_c, for various visual pigments.

Two methods were used for these measurements. In the linear-extrapolation method, marked by "*", λ_{max}/λ_c was determined from the averaged data shown in Text Fig. 1 and 2. λ_c was then calculated from the known λ_{max}, and E_a^P was obtained from $E_a^P = hc/\lambda_c$. In the second method, marked by "#", E_a^P was calculated directly from the same data (as described in **Materials and Methods**) for each of the long wavelengths at which measurements show a temperature-dependence, then averaged, hence the ±SD. λ_c was then obtained from E_a^P with $\lambda_c = hc/E_a^P$, and λ_{max}/λ_c calculated from the known λ_{max}. All E_a^P values in this paper are given in kcal mol^{-1}, obtained by multiplying with Avogadro's number.

Pigment	Chromophore	λ_{max} (nm)	λ_{max}/λ_c*	E_a^{P}* (kcal mol^{-1})	$E_a^{P\#}$ (kcal mol^{-1})	$\lambda_{max}/\lambda_c{}^{\#}$
Mouse S (UV) cone pigment	A_1	360	0.841	66.79	66.27±0.24	0.834
Goldfish blue-sensitive cone pigment	A_2	447	0.838	53.60	53.66±0.14	0.839
Mouse rod pigment	A_1	500	0.840	48.03	47.79±0.57	0.836
Bufo red-rod pigment (rhodopsin)	A_1	500	0.843	48.21	48.08±0.78	0.841
Salamander red-rod pigment (rhodopsin)	A_2/A_1	523	0.830	45.37	47.00±0.34	0.860
Goldfish green-sensitive cone pigment	A_2	537	0.826	44.40	44.45±0.36	0.835
Goldfish red-sensitive cone pigment	A_2	620	0.843	38.88	39.10±0.03	0.848
Mean± SD	--	--	0.837±0.007	--	--	0.842±0.009

Table S2A. Dependence of $f_{\geq E_a^T}$ on α, where $E_a^T = \alpha E_a^P$. Note that m also changes with α because $E_a^T - E_a^{T(app)} = (m-1)RT$.

In each box, the entry in parentheses is E_a^T in kcal mol^{-1}, and underneath is $f_{\geq E_a^T}$. 23°C. Besides testing α values from 0.8 to 1.0, we have, out of curiosity, also examined α > 1 up to 1.2, although it is now generally accepted that α < 1 (see Main Text); nonetheless, the $f_{\geq E_a^T}$ ratios still remain quite similar (table S2B). α < 0.8 is unrealistic. For example, with A$_1$-rhodopsin, α = 0.7 would give E_a^T = 0.7×48.03 kcal mol^{-1} = 33.62 kcal mol^{-1}, which is less than the required minimum of 35 kcal mol^{-1} (see Main Text).

Cell/Pigment	$E_a^T = 0.80 E_a^P$ ($m = 29$) $f_{\geq E_a^T}$	$E_a^T = 0.90 E_a^P$ ($m = 37$) $f_{\geq E_a^T}$	$E_a^T = 0.95 E_a^P$ ($m = 41$) $f_{\geq E_a^T}$	$\boldsymbol{E_a^T = E_a^P}$ ($\boldsymbol{m = 45}$) $f_{\geq E_a^T}$	$E_a^T = 1.05\, E_a^P$ ($m = 50$) $f_{\geq E_a^T}$	$E_a^T = 1.10 E_a^P$ ($m = 54$) $f_{\geq E_a^T}$	$E_a^T = 1.20 E_a^P$ ($m = 62$) $f_{\geq E_a^T}$
Bufo red rod/ A$_1$ *Bufo* rhodopsin	(38.42) 1.59×10^{-7}	(43.23) 9.46×10^{-7}	(45.63) 1.94×10^{-6}	(48.03) 3.65×10^{-6}	(50.43) 1.14×10^{-5}	(52.83) 1.82×10^{-5}	(57.64) 4.01×10^{-5}
Xenopus rod/ A$_2$ *Xenopus* rhodopsin	(36.88) 7.16×10^{-7}	(41.49) 4.31×10^{-6}	(43.80) 8.84×10^{-6}	(46.10) 1.67×10^{-5}	(48.41) 5.03×10^{-5}	(50.71) 8.07×10^{-5}	(55.32) 1.80×10^{-4}
Transgenic mouse rod/ A$_1$ human red cone pigment	(34.50) 6.66×10^{-6}	(38.81) 3.97×10^{-5}	(40.96) 8.15×10^{-5}	(43.12) 1.52×10^{-4}	(45.28) 4.28×10^{-4}	(47.43) 6.82×10^{-4}	(51.74) 1.50×10^{-3}
Transgenic *Xenopus* rod/ A$_2$ human red cone pigment	(31.14) 1.25×10^{-4}	(35.04) 6.87×10^{-4}	(36.98) 1.36×10^{-3}	(38.93) 2.44×10^{-3}	(40.88) 6.03×10^{-3}	(42.82) 9.25×10^{-3}	(46.72) 1.89×10^{-2}
Mouse rod/ A$_1$ mouse rhodopsin	(38.42) 1.59×10^{-7}	(43.23) 9.46×10^{-7}	(45.63) 1.94×10^{-6}	(48.03) 3.65×10^{-6}	(50.43) 1.14×10^{-5}	(52.83) 1.82×10^{-5}	(57.64) 4.01×10^{-5}
Bufo green rod/ A$_1$ *Bufo* blue cone pigment	(44.47) 2.98×10^{-10}	(50.03) 1.55×10^{-9}	(52.81) 2.95×10^{-9}	(55.59) 5.17×10^{-9}	(58.37) 1.74×10^{-8}	(61.15) 2.58×10^{-8}	(66.71) 4.98×10^{-8}

Table S2B. Effect of α on $f_{\geq E_a^T}$ ratios, calculated from Table S2A for the five pairwise comparisons between pigments.

Cell/Pigment	$E_a^T = 0.80E_a^P$ (m = 29)	$E_a^T = 0.90E_a^P$ (m = 37)	$E_a^T = 0.95E_a^P$ (m = 41)	$E_a^T = E_a^P$ (**m = 45**)	$E_a^T = 1.05\ E_a^P$ (m = 50)	$E_a^T = 1.10E_a^P$ (m = 54)	$E_a^T = 1.20E_a^P$ (m = 62)
Bufo red rod/ A$_1$ *Bufo* rhodopsin	$\dfrac{1}{4.5}$	$\dfrac{1}{4.6}$	$\dfrac{1}{4.6}$	$\dfrac{1}{4.6}$	$\dfrac{1}{4.4}$	$\dfrac{1}{4.4}$	$\dfrac{1}{4.5}$
Xenopus rod/ A$_2$ *Xenopus* rhodopsin							
Transgenic mouse rod/ A$_1$ human red cone pigment	$\dfrac{1}{19}$	$\dfrac{1}{17}$	$\dfrac{1}{17}$	$\dfrac{1}{16}$	$\dfrac{1}{14}$	$\dfrac{1}{14}$	$\dfrac{1}{13}$
Transgenic Xenopus rod/ A$_2$ human red cone pigment							
Mouse rod/ A$_1$ mouse rod rhodopsin	$\dfrac{1}{42}$	$\dfrac{1}{42}$	$\dfrac{1}{42}$	$\dfrac{1}{42}$	$\dfrac{1}{38}$	$\dfrac{1}{37}$	$\dfrac{1}{37}$
Transgenic mouse rod/ A$_1$ human red cone pigment							
Xenopus rod/ A$_2$ *Xenopus* rhodopsin	$\dfrac{1}{175}$	$\dfrac{1}{159}$	$\dfrac{1}{154}$	$\dfrac{1}{146}$	$\dfrac{1}{120}$	$\dfrac{1}{115}$	$\dfrac{1}{105}$
Transgenic Xenopus rod/ A$_2$ human red cone pigment							
Bufo green rod/ A$_1$ *Bufo* blue cone pigment	$\dfrac{1}{534}$	$\dfrac{1}{610}$	$\dfrac{1}{658}$	$\dfrac{1}{706}$	$\dfrac{1}{655}$	$\dfrac{1}{705}$	$\dfrac{1}{805}$
Bufo red rod/ A$_1$ *Bufo* rhodopsin							

Table S3. Review of measurements of dark pigment noise in the literature but not used in this paper for comparison with predictions.

Thermal-activation events of rhodopsin can be individually resolved in toad rods, but not as readily in salamander or mammalian rods [but see (*60*)]. Cone pigment activation events in native cones are far too small for direct counting, so an indirect method such as power spectral analysis was used, which suffered from contamination by other phototransduction noise. Thermal-noise rate, instead of rate constant, is listed here when the cellular pigment content is not specified.

Cell/Pigment	Chromophore	λ_{max}	Temperature	Measured Rate Constant (s^{-1}) or Rate (s^{-1} cell^{-1})	Noise-Analysis Method	Source
Bufo green rod/ blue cone pigment	A_1	433 nm	20 °C	0.0065 s^{-1} cell^{-1} *	Probability density histogram	(*61*)
Salamander blue cone/ blue cone pigment	A_2/A_1 (mixture)	Not specified	Not specified	< 2 s^{-1} cell^{-1}	Power spectral analysis	(*62*)
Monkey rod/ rhodopsin	A_1	491 nm	37 °C	5.2×10^{-11} s^{-1}	Direct counting	(*63*)
Bufo red rod/ rhodopsin	A_1	498 nm	~20 °C	~10^{-11} s^{-1}	Direct counting, Power spectral analysis, Probability density histogram	(*45*)
Mouse rod/ rhodopsin	A_1	500 nm	36 °C	0.012 s^{-1} cell^{-1} †	Direct counting	(*47*)
Bullfrog red rod/ rhodopsin	A_1	502 nm	17-19 °C	1.6×10^{-12} s^{-1} ‡	Probability density histogram	(*64*)
	A_2	525 nm	17-19 °C	1.2×10^{-11} s^{-1} ‡		
Salamander red rod/ rhodopsin	A_1	502 nm	21±1 °C	2.13×10^{-12} s^{-1} §	Power spectral analysis	(*17*)
	A_2	528 nm	21±1 °C	7.66×10^{-11} s^{-1} §		
Mouse rod/ green cone pigment	A_1	510 nm	34-37 °C	1.7×10^{-7} s^{-1} ‖	Power spectral analysis	(*65*)
Goldfish green cone/ green cone pigment	A_2	537 nm	Not specified	Not detectable	Power spectral analysis	(*66*)
Monkey red/green cone/ red/green cone pigment	A_1	Not specified	Not specified	2,400 s^{-1} cell^{-1}	Campbell's Theorem	(*67*)
				3,800 s^{-1} cell^{-1}	Campbell's Theorem	(*68*)
Salamander red cone/ red cone pigment	A_2/A_1 (mixture)	Not specified	Not specified	600±200 s^{-1} cell^{-1}	Power spectral analysis	(*62*)
		Not specified	23 °C	5.7×10^{-6} s^{-1}	Power spectral analysis	(*69*)

* This rate is ~200 times higher than what we report here (0.0003 s^{-1} cell^{-1} at 23°C; see Main Text). We are unable to offer an explanation for this large disparity, except pointing out that the unitary responses we observed were well resolved from background noise (Text Fig. 3).

† This rate is essentially the same as previously found by us [0.013 s^{-1} cell^{-1} at 37°C (*46*)].

‡ A_1 and A_2 bullfrog rhodopsins are from the ventral retina and the dorsal retina, respectively. No temperature-dependence was provided for rate-estimation at 23°C, but their A_1 rhodopsin/A_2 rhodopsin rate-ratio of 1/7.5 is similar to ours (1/9; see Text Table 1).

§ The A_1 rhodopsin/A_2 rhodopsin noise rate is 1/36, which is 4-fold smaller than what we found. This could partly be due to the apparently substantial difference in λ_{max} between salamander and *Xenopus* A_2 rhodopsins.

‖ This rate constant is 22-fold higher than what our theory would predict. Despite this being a study of mouse green cone pigment in rods, the dark events were below resolution; accordingly, only the less-direct approach of power spectral analysis was used.

22

Table S4. The pre-exponential factor, *A,* for different visual pigments.

The pre-exponential factor, *A,* for different visual pigments was calculated based on: noise rate constant $= A \times f_{\geq E_a^T}$ (see Text Table 1). The average cone- and rod-pigment *A* values are used in Fig. 4C and fig. S8; and their ratio (~26) is used to adjust for the difference in *A* value between cone and rod pigments in noise comparisons.

Pigments		A (s^{-1})	Average A (s^{-1}) (Mean ± SD)
Rod pigments	A$_1$ *Bufo* rhodopsin	1.15×10^{-6}	$7.19(\pm 9.55) \times 10^{-6}$
	A$_1$ mouse rhodopsin	1.82×10^{-5}	
	A$_2$ *Xenopus* rhodopsin	2.22×10^{-6}	
Cone pigments	A$_1$ human red cone pigment	2.72×10^{-4}	$1.88(\pm 1.47) \times 10^{-4}$
	A$_2$ human red cone pigment	2.75×10^{-4}	
	A$_1$ *Bufo* blue cone pigment	1.82×10^{-5}	

Table S5. Pigment-content calculations.

Rod outer segment dimensions are given as diameter × length. In all calculations below, the pigment concentration in the outer segment is assumed to be 3.5 mM (*19*). The cell dimensions are not exact. In particular, the mouse rod outer segment is too tiny for precise determination of its diameter and the length of the outer segment under recording by the pipette.

Note: With *Bufo* red rods, Baylor *et al.* (*45*) previously estimated the thermal-activity rate constant for A_1 rhodopsin to be $\sim 10^{-11}$ s^{-1} at 20°C, based on the number of pigment molecules in the portion of the outer segment under recording being 2.0×10^9. If the calculations were made by using a 3.5 mM pigment concentration, their rate constant would be 7.6×10^{-12} s^{-1}, which is closer to our present value of 4.18×10^{-12} s^{-1} (Text Table 1).

Cell/Pigment	Source	Recorded part of outer segment
Bufo red rod/ A_1 *Bufo* rhodopsin	This work	Dimensions: 7.5 × 65.0 μm Volume = 2870 μm^3 Pigment molecules = 6.0×10^9
Xenopus rod/ A_2 *Xenopus* rhodopsin	(*59*)	Dimensions: 6.4×40 μm Volume = 1286 μm^3, Pigment molecules = 2.7×10^9
Transgenic mouse rod/ A_1 human red cone pigment	(*46*) and this work	1% (based on spectral shift) of total pigment content (see below) Pigment molecules = 6.5×10^5
Transgenic *Xenopus* rod/ A_2 human red cone pigment	(*59*)	0.03% (based on spectral shift) of total pigment content (see above) Pigment molecules = 8.1×10^5
Mouse rod/ A_1 mouse rhodopsin	(*46*) and this work	Dimensions: 1.4×20 μm Volume = 31 μm^3 Pigment molecules = 6.5×10^7
Bufo green rod/ A_1 *Bufo* blue cone pigment	This work	Dimensions: 7.3×37 μm, Volume = 1548 μm^3 Pigment molecules = 3.3×10^9

References

1. C. F. Goodeve, *Proc. Roy. Soc. A* **155**, 664 (1936).

2. D. R. Griffin, R. Hubbard, G. Wald, *J. Opt. Soc. Am.* **37**, 546 (1947).

3. W. S. Stiles, in *Transactions of the Optical Convention of the Worshipful Company of Spectacle Makers*. (Spectacle Makers' Company, London, 1948), pp. 97-107.

4. E. J. Denton, M. H. Pirenne, *J. Physiol.* **125**, 181 (1954).

5. P. R. Lewis, *J. Physiol.* **130**, 45 (1955).

6. T. D. Lamb, *Vision Res.* **35**, 3083 (1995).

7. H. De Vries, *Experientia* **4**, 357 (1948).

8. R. C. C. St. George, *J. Gen. Physiol.* **35**, 495 (1952).

9. R. Srebro, M. Behbehani, *J. Physiol.* **224**, 349 (1972).

10. T. D. Lamb, *J. Physiol.* **346**, 557 (1984).

11. D. A. Baylor, G. Matthews, K. W. Yau, *J. Physiol.* **337**, 723 (1983).

12. P. Ala-Laurila, P. Saarinen, R. Albert, A. Koskelainen, K. Donner, *Vis. Neurosci.* **19**, 781 (2002).

13. T. Yoshizawa, G. Wald, *Nature* **212**, 483 (1966).

14. Y. Tsukamoto, S. Horiuchi, T. Yoshizawa, *Vision Res.* **15**, 819 (1975).

15. F. I. Harosi, *Vision Res.* **34**, 1359 (1994).

16. V. J. Kefalov *et al.*, *Neuron* **46**, 879 (2005).

17. P. Ala-Laurila, K. Donner, R. K. Crouch, M. C. Cornwall, *J. Physiol.* **585**, 57 (2007).

18. C. D. Bridges, *Vision Res.* **7**, 349 (1967).

19. F. I. Harosi, *J. Gen. Physiol.* **66**, 357 (1975).

20. C. L. Makino, M. Groesbeek, J. Lugtenburg, D. A. Baylor, *Biophys. J.* **77**, 1024 (1999).

21. M. C. Cornwall, G. J. Jones, V. J. Kefalov, G. L. Fain, H. R. Matthews, *Methods Enzymol.* **316**, 224 (2000).

22. A. G. Palacios, F. J. Varela, R. Srivastava, T. H. Goldsmith, *Vision Res.* **38**, 2135 (1998).

23. G. Shi, K. W. Yau, J. Chen, V. J. Kefalov, *J. Neurosci.* **27**, 10084 (2007).

24. J. Lem *et al.*, *Proc. Natl. Acad. Sci. U. S. A.* **96**, 736 (1999).

25. D. G. Luo, K. W. Yau, *J. Gen. Physiol.* **126**, 263 (2005).

26. S. S. Nikonov, R. Kholodenko, J. Lem, E. N. Pugh, Jr., *J. Gen. Physiol.* **127**, 359 (2006).

27. R. Srebro, *J. Physiol.* **187**, 417 (1966).

28. A. Koskelainen, P. Ala-Laurila, N. Fyhrquist, K. Donner, *Nature* **403**, 220 (2000).

29. P. Ala-Laurila, J. Pahlberg, A. Koskelainen, K. Donner, *Vision Res.* **44**, 2153 (2004).

30. M. Karplus, J. A. McCammon, *Nat. Struct. Biol.* **9**, 646 (2002).

31. K. Palczewski *et al.*, *Science* **289**, 739 (2000).

32. L. M. Frutos, T. Andruniow, F. Santoro, N. Ferre, M. Olivucci, *Proc. Natl. Acad. Sci. U. S. A.* **104**, 7764 (2007).

33. J. A. Gascon, V. S. Batista, *Biophys. J.* **87**, 2931 (2004).

34. S. Hayashi, E. Tajkhorshid, K. Schulten, *Biophys. J.* **96**, 403 (2009).

35. M. G. Khrenova, A. V. Bochenkova, A. V. Nemukhin, *Proteins* **78**, 614 (2010).

36. J. Saam, E. Tajkhorshid, S. Hayashi, K. Schulten, *Biophys. J.* **83**, 3097 (2002).

37. A. Strambi, P. B. Coto, L. M. Frutos, N. Ferre, M. Olivucci, *J. Am. Chem. Soc.* **130**, 3382 (2008).

38. D. Fotiadis *et al.*, *Curr. Opin. Struct. Biol.* **16**, 252 (2006).

39. M. Schreiber, M. Sugihara, T. Okada, V. Buss, *Angew. Chem. Int. Ed. Engl.* **45**, 4274 (2006).

40. A. Cooper, *Nature* **282**, 531 (1979).

41. J. A. Gascon, V. S. Batista, *Biophys. J.* **87,** 2931 (2004).

42. C. N. Hinshelwood, *The kinetics of chemical change*. (The Clarendon press, Oxford, 1940), pp. 39 and 79.

43. P. Ala-Laurila, K. Donner, A. Koskelainen, *Biophys. J.* **86**, 3653 (2004).

44. P. W. Atkins, J. De Paula, *Physical Chemistry*. (Oxford University Press, New York, ed. 8th, 2006).

45. D. A. Baylor, G. Matthews, K. W. Yau, *J. Physiol.* **309**, 591 (1980).

46. Y. Fu, V. Kefalov, D. G. Luo, T. Xue, K. W. Yau, *Nat. Neurosci.* **11**, 565 (2008).

47. M. E. Burns, A. Mendez, J. Chen, D. A. Baylor, *Neuron* **36**, 81 (2002).

48. O. Hisatomi, Y. Takahashi, Y. Taniguchi, Y. Tsukahara, F. Tokunaga, *FEBS Lett.* **447**, 44 (1999).

49. J. Ma, S. Znoiko, K. L. Othersen, J. C. Ryan, J. Das *et al.*, *Neuron* **32**, 451 (2001).

50. Y. Takahashi, O. Hisatomi, S. Sakakibara, F. Tokunaga, Y. Tsukahara, *FEBS Lett.* **501**, 151 (2001).

51. D. Hicks, R. S. Molday, *Exp. Eye Res.* **42**, 55 (1986).

52. J. W. Mandell, P. R. MacLeish, E. Townes-Anderson, *J. Neurosci.* **13**, 3533 (1993).

53. G. Matthews, *J. Physiol.* **342**, 347 (1983).

54. D. A. Baylor, T. D. Lamb, K. W. Yau, *J. Physiol.* **288**, 613 (1979).

55. V. I. Govardovskii, N. Fyhrquist, T. Reuter, D. G. Kuzmin, K. Donner, *Vis. Neurosci.* **17**, 509 (2000).

56. T. Okada, O. P. Ernst, K. Palczewski, K. P. Hofmann, *Trends Biochem. Sci.* **26**, 318 (2001).

57. R. A. Mathies, Novartis Found. Symp. **224**,70 (1999).

58. D. Polli et al., Nature **467**, 440 (2010).

59. V. Kefalov, Y. Fu, N. Marsh-Armstrong, K. W. Yau, *Nature* **425**, 526 (2003).

60. T. Doan, A. Mendez, P. B. Detwiler, J. Chen, F. Rieke, *Science* **313**, 530 (2006).

61. G. Matthews, *J. Physiol.* **349**, 607 (1984).

62. F. Rieke, D. A. Baylor, *Neuron* **26**, 181 (2000).

63. D. A. Baylor, B. J. Nunn, J. L. Schnapf, *J. Physiol.* **357**, 575 (1984).

64. K. Donner, M. L. Firsov, V. I. Govardovskii, *J. Physiol.* **428**, 673 (1990).

65. K. Sakurai *et al.*, *J. Gen. Physiol.* **130**, 21 (2007).

66. D. Holcman, J. I. Korenbrot, *J. Gen. Physiol.* **125**, 641 (2005).

67. J. L. Schnapf, B. J. Nunn, M. Meister, D. A. Baylor, J. Physiol. **427**, 681 (1990).

68. D. M. Schneeweis, J. L. Schnapf, *J. Neurosci.* **19**, 1203 (1999).

69. A. P. Sampath, D. A. Baylor, *Biophys. J.* **83**, 184 (2002).